Global distribution of light (photosynthetically active radiations) reaching the sea floor

Jean-Pierre Gattuso[1, 2], Bernard Gentili[1], David Antoine[1, 3], and David Doxaran[1]

[1]Sorbonne Université, CNRS, Laboratoire d'Océanographie de Villefranche, 181 chemin du Lazaret, F-06230 Villefranche-sur-mer, France
[2]Institute for Sustainable Development and International Relations, Sciences Po, 27 rue Saint Guillaume, F-75007 Paris, France
[3]Remote Sensing and Satellite Research Group, Curtin University, Perth, Western Australia, 6845, Australia

Correspondence: J.-P. Gattuso (gattuso@obs-vlfr.fr)

Abstract.

A 20-year (1998–2016) continuous monthly data set of the global distribution of light (photosynthetically active radiations) reaching the seabed is presented. It builds on a previous data set (Gattuso et al., 2006), using ocean color and bathysmetric data to estimate benthic irradiance, while offering critical improvements. The time series is 4 times longer (20 vs 5 years), the spatial resolution is twice better (4.6 vs 9.3 km at the equator) and the bathymetric resolution is 8 times better (0.46 vs 3.7 km at the equator). The paper describes the theoretical and methodological basis for all data processing. This new product is used to estimate the surface area of the sea floor where light does not limit the distribution of benthic organisms and communities. The complete data set is provided as 14 netCDF files available on Pangaea (textbfURL). The R package CoastalLight, available on Github (https://github.com/jpgattuso/CoastalLight.git) allows calculations of the surface area that receives more than a given threshold of irradiance in three regions (non polar, Arctic and Antarctic) and get various geographical and optical data from a remotely and freely accessible server.

1 Introduction

Light is a key ocean variable. It shapes the composition of benthic and pelagic communities by controlling the three-dimensional distribution of primary producers, the lowest levels of the wood webs. Light also plays a major role in the global carbon cycle by controlling primary production, the main source of new organic carbon in the ocean (Assis et al., 2018). In the marine environment, sunlight is rapidly absorbed by the water column and primary production is restricted to the shallow photic zone above 200 m depth (except for localized chemo-autotrophic communities). Marine diazotrophs, which fix dinitrogen into organic forms, are also light-dependent. Furthermore, many marine ecosystem engineers require light because they are either

plants (mangrove, saltmarshes, seagrass, coralline algae) or animals living in symbiosis with endosymbiotic algae (e.g., some mollusks and zooxanthellate, reef-building corals).

Until the late 1970s, most water transparency measurements were performed using Secchi disks (Tyler, 1968) and several formulations became available to ... (e.g., Weinberg, 1976). Remote sensing observations of ocean color showed great promise as early as 1978, when the coastal zone color scanner (CZCS) was launched. It was followed by several other instruments on-board satellites. Ocean color measurements of the Sea-Viewing Wide Field-of-View Sensor (SeaWIFS), launched in 1997, are used to derive the concentration of chlorophyll-a (C_{sat}) and the mean attenuation coefficient for PAR (K_{PAR}). Until 2006, most attention was focused on the light field in the water column to derive open-ocean primary production (e.g., Antoine et al., 1996). However, primary production also occurs in the coastal ocean when enough light reaches the sea floor. For example, on coral reefs, benthic primary production can represent 90% of the total primary production (Delesalle et al., 1993). Primary production in coastal vegetated habitats such as mangroves, seagrass beds and tidal marshes, the so-called 'blue carbon ecosystems', has recently received considerable interest in the past 10 years. due to their disproportionately large contribution to global carbon sequestration (Macreadie, 2019). It has been recently suggested that benthic macroalgae also contribute to global carbon burial Krause-Jensen et al. (2018).

Gattuso et al. (2006) used satellite (SeaWiFS) data collected between 1998 and 2003 to estimate, for the first time at a nearly global scale, the irradiance reaching the bottom of the coastal ocean. They provided cumulative functions to estimate the percentage of the surface (S) of the coastal zone receiving an irradiance greater than some irradiance level. These data were used to investigate the extent of macroalgae (Krause-Jensen and Duarte, 2016), restoration of seagrass ecosystems (Eriander, 2017), role of vegetated coastal habitats in the ocean carbon budget (Duarte, 2017), macroalgal subsidies supporting benthic invertebrates (Filbee-Dexter and Scheibling, 2015), global continental shelf denitrification (Eyre et al., 2013), and benthic primary production in the Arctic Ocean (Attard et al., 2016; Glud et al.).

More recently, Assis et al. (2018) provided a data layer for benthic irradiance for species distribution modelling as part of the Bio-ORACLE set of GIS rasters. This data set is based on K_{d490} in contrast to Gattuso et al. (2006) who used the more appropriate $K_{d\ PAR}$ [**Davids: Correct? que peut-on dire d'autre?**]

Since these first efforts, new products have become available which can improve estimates of the global distribution of benthic irradiance. These include a much longer time series of ocean color (20 vs 5 years) with an improved spatial resolution (4.6 vs 9.3 km at the equator). Bathymetric data have also considerably improved since 2006 (0.46 vs 3.7 km at the equator). Here we make use of these new products to provide global distribution of light (photosynthetically active radiations) reaching the seabed.

2 Methods

The characteristics of the products used by Gattuso et al. (2006) and by the present study are summarized and compared in Table 1 .

Table 1. Main characteristics of the products used by Gattuso et al. (2006) and by the present study.

	Gattuso et al. (2006)	Present study
Satellite	SeaWiFS	1998 to June 2002: SeaWiFS
		Jul. 2002 to Dec; 2010: SeaWiFS + MODIS
		Jan. 2011 to Jan. 2012: MODIS
		Feb. 2012 to 2018: MODIS and VIIRS
Coverage	1998 to 2003	1998 to 2018
Sat. resolution	$\approx 1/12^\circ$ = 9.3 km at equator	$\approx 1/24^\circ$ = 4.6 km at equator
Bathymetry	ETOPO 2 min	GEBCO 15 sec
	3.7 km at equator	0.46 km at equator
Data	PAR, C_{sat}, $nLw(555)$, K_d from C_{sat}	PAR, K_{PAR}, C_{sat}, $R_{rs}(555)$

2.1 Remote sensing data

Monthly Level-3 of PAR and K_{PAR}, C_{sat}, and $R_{rs}(555)$ of SeaWiFS, MODIS, MERIS, VIIRS data were obtained from the European Service for Ocean Colour (http://www.globcolour.info). The resolution is 1/24°. Together, the 252 monthly images downloaded cover the period 1998 to 2018.

2.2 Bathymetry and coastline

Surface areas and average depths were estimated from the 2019 General Bathymetric Chart of the Oceans (GEBCO; https://www.gebco.net) gridded bathymetry data (1/240°resolution) using the Generic Mapping Tools (GMT; Wessel et al., 2013). The coastline was from the Global Self-consistent, Hierarchical, High-resolution Geography (GSHHG) as implemented in GMT. The full resolution was used. The Arctic, Antarctic, and non-polar regions represent, respectively, 24.1%, 0.6%, and 75.3% of the total coastal surface covered (depth < 200 m).

2.3 Case 1 versus Case 2 waters

It is beyond the scope of this paper to review the criteria used to eliminate dubious data when generating a Level-3 composite, except for discriminating the water type as either Case 1 or Case 2 waters (Morel and Prieur, 1977). In Case 1 waters, where phytoplankton is the main contributor to attenuation (but see Claustre and Maritorena, 2003), it is generally assumed that K_{PAR} is related to the concentration of chlorophyll-a, itself derived from reflectance values. The situation is, however, not as straightforward in Case 2 waters where light attenuation by colored dissolved organic matter and suspended particles other than phytoplankton can be significant, which often happens in coastal waters. The discrimination between these two types is performed at the Level-2 in the processing, yet it is not considered when generating the Level-3 composites (B. Franz, personal communication, September 2019). Therefore, the average chlorophyll-a concentration C_{sat} in a given bin of a Level-3 composite may have been computed over any proportion of Case 1 and Case 2 waters.

The accuracy of C_{sat} in Case 1 waters is claimed to be $\pm 30\%$ whereas its is unknown in Case 2 waters. It is therefore not possible to estimate the accuracy of the chlorophyll product in coastal areas and, in turn, the accuracy of the diffuse attenuation coefficient. We apply an *a posteriori* determination of the water type based on the average C_{sat} and $R_{rs}(555)$, the remote sensing reflectance at 555 nm (see below), which is not based on specific algorithms for each water type since no universal algorithm exists. This determination nevertheless provides an indication of bins of Case 2 water because, on average, the individual pixels in the bins were predominantly of the Case 2 type. Waters with a C_{sat} value lower than 0.2 mg m^{-3} are considered to be Case 1 waters (A. Morel, personal communication; **à formuler différemment car il est décédé depuis longtemps maintenant**). When C_{sat} is higher than 0.2 mg m^{-3}, the identification of turbid Case 2 waters is performed as in Morel and Bélanger (2006) by comparing the water reflectance at 555 nm ($R(555)$) to the maximum value it should have in Case 1 waters ($R_{lim}(555)$). Turbid Case 2 waters are those for which $R(555) > R_{lim}(555)$. To perform this test, $R_{rs}(555)$ is converted into $R(555)$ as follows (Morel and Gentili, 1996):

$$R(555) = R_{rs}(555) \times Q_0(555)/\mathfrak{R}_0 \tag{1}$$

where $Q_0(555)$ is the chlorophyll-dependent Q-factor, i.e., the ratio of the upward irradiance to the upwelling radiance (Morel et al., 2002), and $\mathfrak{R}_0$ is a term which merges all reflection and refraction effects at the air-sea interface (0.529). Since $R_{rs}(555)$ is fully normalized (Morel and Gentili, 1996), its dependence on the viewing angle and the sun zenith angle are removed so that both Q and $\mathfrak{R}$ are taken for a nadir view and a sun at zenith (hence the "0" subscript).

2.4 Benthic irradiance

The diffuse attenuation coefficient for the downwelling irradiance $K_d(\lambda_0)$ for a given wavelength λ_0 describes the exponential propagation of irradiance with depth in the water column. It determines the amount of radiation reaching a given depth:

$$K_d(\lambda_0, z) = \frac{-\partial \ln(E_d(\lambda_0, z))}{\partial z} \tag{2}$$

The spectral composition of the radiation is not considered in this work and only its integral value between 400 and 700 nm is used (i.e., the photosynthetically available radiation, PAR). The mean attenuation coefficient for PAR is therefore:

$$K_{PAR}(z) = \frac{-d \ln(PAR(z))}{dz} \tag{3}$$

The average value $\overline{K}_{PAR}$ of $K_{PAR}(z)$ over the euphotic zone, i.e., that depth where PAR is reduced to 1% of its value just beneath the sea surface, is computed from the corresponding chlorophyll concentration for case 1 waters C_{sat} and $\overline{K}_d(490)$ using the following equations (Morel et al., 2007; ACRI-ST GlobColour Team, 2017) :

$$\overline{K}_d(490) = 0.0166 + 0.08349 \times C_{sat}^{0.63303} \quad (4)$$

$$\overline{K}_{PAR} = 0.0665 + 0.874 \times \overline{K}_d(490) - 0.00121/\overline{K}_d(490) \quad (5)$$

The bottom irradiance is then calculated:

$$PAR_{bottom} = \exp(-\overline{K}_{PAR} \times z) \quad (6)$$

- for the Non-Polar region all months are taken into account, so we have 21 years $\times$ 12 months = 252 values by pixel
- for the Arctic region months 6-10 (June to October) are taken into account, so we have 21 years $\times$ 5 months = 105 values by pixel
- for the Antarctic region months 1-3 and 11-12 (January to March and November-December) are taken into account, so we have 21 years $\times$ 5 months = 105 values by pixel
- in fine, we have 252 monthly images of PAR_{bottom} for the **NonPolar** region and 105 for the**Arctic** region.

The product delivered comprises longitude, latitude, depth, area, PAR, $\overline{K}_{PAR}$, PAR_{bottom} for each pixel. PAR, $\overline{K}_{PAR}$ and PAR_{bottom} are monthly climatologies or a climatology over the entire time series. The calculation of surface area receiving a light above a certain threshold does not use these climatologies (see next section). [Move text from below]

2.5 Surface area receiving light above a certain threshold

Calculations of surface area receiving a light above a certain threshold are made in two steps. First a $\mathcal{P}$-function is calculated with the available pixels; then the area is calculated as the product of the $\mathcal{P}$-function by the surface of the coastal zone ([0-200 m].

2.5.1 The three main regions

A region is a piece of the Earth, defined by an interval of longitude and an interval of latitude. Earth is not homogeneously covered by the satellites. In polar zones, data are not available several months a year. So three mean regions have been defined:

- the "NonPolar" region $[60°S; 60°N]$, where data are always available,
- the "Arctic" region $[60N; 90N]$, where data are available during the months of June, July, August, September, and October,
- the "Antarctic" region $[-90°S; -60°S]$, where data are available during the months of January, February, March, November, and December.

Surface areas are calculated for these three regions by restricting monthly satellite images to their respective periods and geographic limitations.

2.5.2 $\mathcal{P}$-functions

Definition of a $\mathcal{P}$-function for a monthly PAR_{bottom} image of a region

- let I be the the monthly image (values of PAR_{bottom} on the floor of the coastal zone of the region)
- let $S_{a,I}$ be the available surface, i.e. the total surface of pixels for which an irradiance value is available (varying from one month to another according irradiance satellite images);
- let E a value of irradiance (expressed in $\mathrm{mol\ photons\ m^{-2}\ d^{-1}}$);
- let $s_I(E)$ the total surface of pixels collecting irradiance greater than E;
- the $\mathcal{P}_I$-function if defined as $\mathcal{P}_I(E) = 100 s_I(E)/S_{a,I}$

Definition of a climatologic $\mathcal{P}$-function

Our purpose is now to define a $\mathcal{P}$-function for a set of monthly images $\mathcal{I} = \{I_i, i = 1 \dots n\}$. Giving a value of irradiance E, it is defined as :

$$\mathcal{P}_{\mathcal{I}}(E) = 100 \sum_{i=1}^{n} s_{I_i}(E) / \sum_{i=1}^{n} S_{a,I_i} \tag{7}$$

Climatologic monthly $\mathcal{P}$-function

In this case a month is selected; the 21 images of this month (from 1998 to 2018) are selected to calculate the $\mathcal{P}$-function according to equation 7. So we have :

- 12 climatologic monthly $\mathcal{P}$-function for the Non-Polar region,
- 5 climatologic monthly $\mathcal{P}$-function for the Arctic region,
- 5 climatologic monthly $\mathcal{P}$-function for the Antarctic region.

Climatologic global $\mathcal{P}$-function

$\mathcal{P}_g$ is obtained, using all images (252 for Non-Polar and 105 for Arctic and Antarctic) in equation 7.

$\mathcal{P}$-functions for a subregion

Within one of the three main regions, a subregion may be defined; in this case images are cropped according to the subregion's boundaries, and the months used are those of the main region. Calculation is identical to that described above for climatological global $\mathcal{P}$-function (section 2.5.2).

2.5.3 Surface areas

Let $\mathcal{P}$ be the $\mathcal{P}$-function of the zone and S_{geo} its area : the area receiving irradiance above a threshold E is :

$$s(E) = S_{geo}\,\frac{\mathcal{P}(E)}{100} \tag{8}$$

3 Results and discussion

The present study essentially confirms the bathymetric data reported in our earlier study (Gattuso et al., 2006) but provides some substantial differences on the optical data.

3.1 Surface area and depth of sub-regions of the ocean

Table 2. Surface area (S) of coastal waters (depth $<$ 200 m) of different optical characteristics. Calculations were performed on monthly images. Values reported by Gattuso et al. (2006) are shown in parentheses for comparative purposes. Gattuso et al. (2006) did not report data for the Antarctic.

	Arctic		Antarctic		Non Polar	
	$S(10^6 km^2)$	$S(\%)$	$S(10^6 km^2)$	$S(\%)$	$S(10^6 km^2)$	$S(\%)$
Coastal Zone	6.1 (6.13)	100 (100)	0.146	100	19.1 (18.8)	100 (100)
Case 1	2.05 (1.6)	33.6 (26.2)	0.024	16.4	10.2 (8.47)	53.3 (45)
Case 2	1.03 (0.81)	16.9 (13.2)	0.027	18.5	5.74 (6.76)	30.1 (35.9)
Case 1 and Case 2	3.08 (2.41)	50.5 (39.40)	0.051	34.9	15.9 (15.23)	83.4 (80.9)

The area and depth of the three regions measured with the most recent GEBCO bathymetry are very similar to those obtained with the coarser ETOPO2 data set used by Gattuso et al. (2006) (Table 2). The surface area of the ocean with less than 200 m depth is 25.3 10^6 km^2. Three geographical areas are considered: the Arctic (60 to 90°N), non polar (60°N to 60°S), and Antarctic (60 to 90°S) regions, respectively covering 24.1, 75.5 and 0.6% of the global coastal zone. The average depth in these regions is, respectively, 77.3, 137 and 71.3 m. The average depth of the coastal zone is almost twice as large in the Antarctic than in the Arctic and non polar regions (137 vs 77 and 71 m).

3.2 Availability of ocean colour data and seawater types

The availability of ocean color data on monthly images is highly variable depending on the latitude and month of the year (Fig. 1). It is highest in non polar regions where, on average, data are available in 83% (range: 62-96%) of the pixels in monthly images. There is light for only 5 summer months of the year in the Arctic (June to October) and Antarctic (November to March). During these periods, data availability is higher in mid-summer than in early- and late summer (Fig. 1). Data availability also decreases as one gets closer to the poles. On average, data are available for 51 and 35% of the summer images in the Arctic and

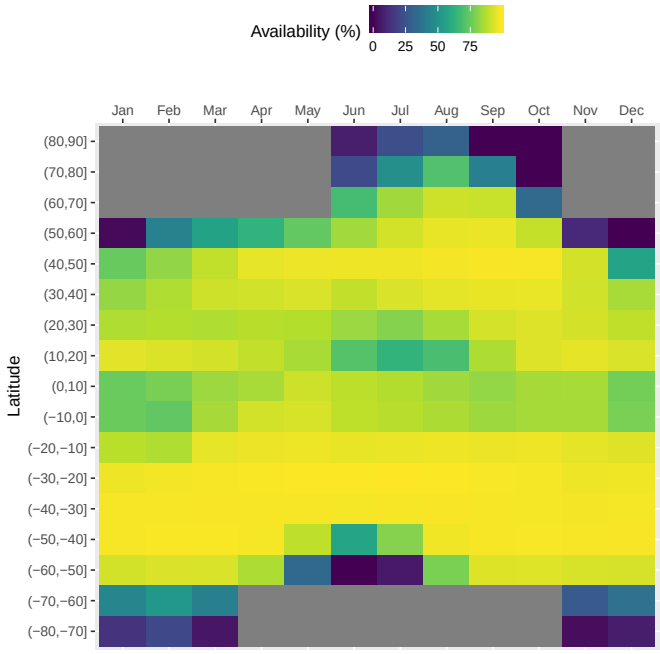

Figure 1. Mean monthly availability of remote sensing data over the entire 21 years time-series expressed as the percent of the surface of the coastal zone in each latitudinal band.

Antarctic regions (ranges: 6-89% and 11-58%, respectively; 3). It is higher in the present study which used multiple sensors than in a previous study that only used SeaWiFS data (Gattuso et al., 2006). Two factors contribute to the low availability of data in polar regions: high occurrence of cloudy days and low incidence of the sun [**Les Davids**: merci de préciser et compléter]

The coverage of the Arctic has improved with about 20% more pixels with available data 3. Case 1 and Case 2 waters are approximately equally distributed in the Antarctic region (Table 2). In contrast, the distribution of Case 1 and Case 2 waters in the non polar region, with a clear dominance of Case 1 over Case 2 waters (64 vs 36%) in the present study whereas it was more even in Gattuso et al. (2006, 55 vs 45%). This difference mzay be due to the different approach used to differentiate Case 1 and Case 2 waters. The present study used the remote sensing reflectance at 555 nm ($R_{rs}(555)$) provided by the European Service for Ocean Colour whereas it was roughly estimated ... in the previous study (Gattuso et al., 2006) [**Bernard**]. The quality of the results should therefore be improved. In any case, the usefulness of this distinction is relatively limited because the light penetration through the water column is calculated in the same way in the two cases. The distribution of water quality is however useful to estimate the reliability of the bottom irradiance which is much better in Case 1 waters than in Case 2 waters.

Table 3. Surface area and average depth of the various pixel classes. Calculations were performed on monthly images for the periods indicated. Values reported by Gattuso et al. (2006) are shown in parentheses for comparative purposes. Gattuso et al. (2006) did not report data for the Antarctic. $Z_{1\%}$ is the depth at which benthic irradiance equals 1% of surface irradiance. Available pixels are the pixels for which PAR, K_{PAR}, C_{sat}, and $R_{rs}(555)$ are available for analysis. **Bernard: Add average depth of missing pixels**.

	Arctic (June-October)			Antarctic (November-March)			Non Polar (January-December)		
	Min	Max	Mean	Min	Max	Mean	Min	Max	Mea
Available/Total number of pixels	0.059 (0.20)	0.89 (0.60)	0.51 (0.39)	0.11	0.58	0.35	0.62 (0.68)	0.96 (0.90)	0.83 (0
Average depth available pixels (m)	66 (74)	103 (87)	82 (80)	148	131	140	76 (67)	67 (71)	72 (6
Case 1 pixels/available pixels	0.53 (0.58)	0.8 (0.72)	0.67 0.66)	0.25	0.68	0.47	0.55 (0.46)	0.7 (0.65)	0.64 (0
Average depth Case 1 pixels (m)	84 (86)	120 (99)	97 (93)	158	143	150	91 (80)	82 (86)	87 (8
Case 2 pixels/available pixels	0.2 (0.28)	0.47 (0.42)	0.33 (0.34)	0.32	0.75	0.53	0.3 (0.35)	0.45 (0.54)	0.36 (0
Average depth Case 2 pixels (m)	39 (43)	67 (70)	50 (55)	144	111	131	52 (44)	37 (57)	44 (5
$Z < Z_{1\%}$ pixels/available pixels	0.07	0.21	0.15	0.01	0.07	0.03	0.27	0.36	0.31

3.3 Bottom irradiance

The distribution of PAR_{bottom} has changed in the present study compared to the previous one of Gattuso et al. (2006), with less irradiance values above 0.2 $\text{mol photons m}^{-2}\ \text{d}^{-1}$ and more irradiance values around 0.1 $\text{mol photons m}^{-2}\ \text{d}^{-1}$ in 2019 than in 2006 (Fig. 2). Consequently, the surface area receiving irradiance above a certain threshold also declined (Fig. 3).

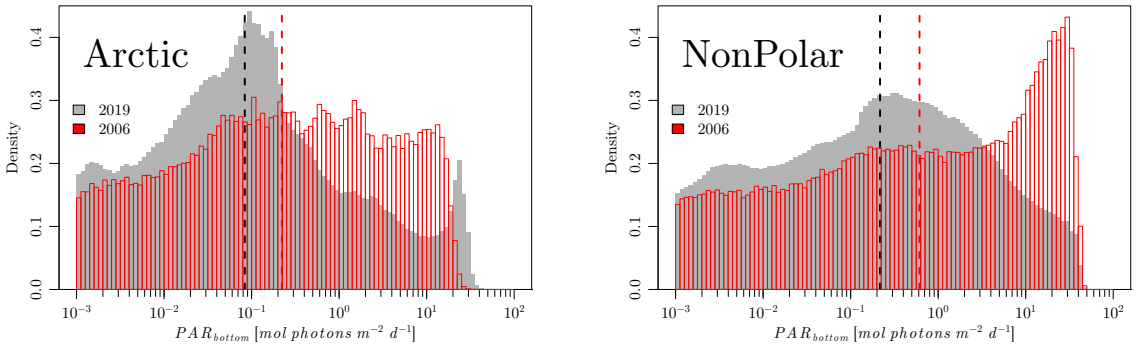

Figure 2. Distribution of PAR_{bottom} in the present study (2019) and in Gattuso et al. (2006). **Bernard: median or mean? Je pense median c'est mieux**

The surface area of the sea floor receiving an irradiance larger than a threshold value is lower than with the previous estimate of Gattuso et al. (2006)(Fig. 3). Differences are low below an irradiance threshold of 0.2 $\text{mol photons m}^{-2}\ \text{d}^{-1}$: 3 to 16% lower, respectively in the non polar and Arctic regions. However, differences are as high as 26 and 56%, respectively in the non

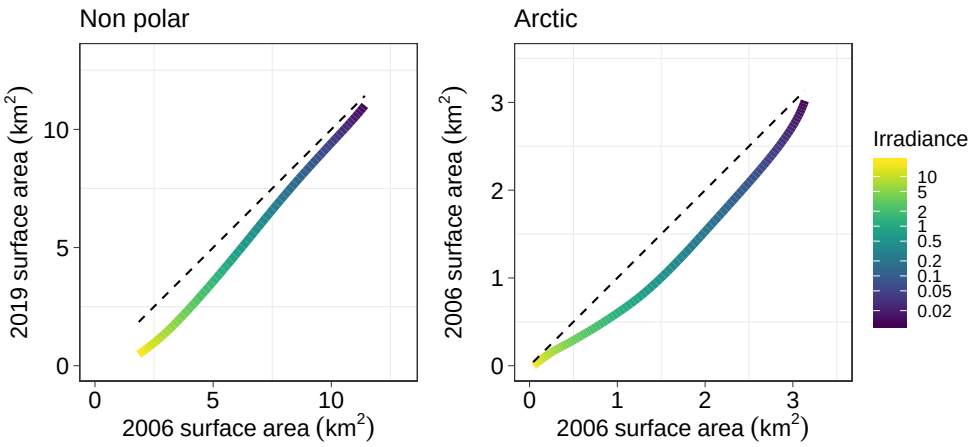

Figure 3. Comparison of the surface area of the sea floor receiving an irradiance larger than a threshold value ranging from 0.01 to 20 $\mathrm{mol\ photons\ m^{-2}\ d^{-1}}$ calculated in the present paper compared with the surface area reported in 2006 by Gattuso et al. (2006). The dotted line is the 1:1 relationship.

polar and Arctic regions for irradiance thresholds ranging between 10 and 50 $\mathrm{mol\ photons\ m^{-2}\ d^{-1}}$. Such differences can be due to several causes.

~~The quality of data on the surface area receiving irradiance above a certain threshold also depends on two factors. The area is calculated on pixels for which data are available and is extended to the surface area of the whole region or sub-region considered. This assumes that the light penetration in the missing pixels is similar to that of the available pixels. The availability of data on the monthly images of ocean color is therefore a key criterion to assess the uncertainty. It is lower in polar regions, where only 35 to 51% of the pixels have data, than in non polar regions where the mean data availability is 81%. The second factor is the distribution of water qualities as explained above.~~

The present study and the one of Gattuso et al. (2006) used different approaches. In the 2006 study, one p-function was derived for each month and then monthly means calculated, implicitly giving the same weight to each month, irrespective of the number of pixels with available data. In the present study, each month has a weight proportional to the surface area for which data are available, hence providing better estimates. Second, there are more data available in the data set compiled in the present paper, especially in the Arctic [**Question aux Davids: est ce que les capteurs qui ont succédé à SeAWiFS "voient" mieux**

l'Arctique?]. Third, Gattuso et al. (2006) fitted polynomial function on the relationship between irradiance and the cumulative surface area of the sea floor receiving irradiance above a prescribed threshold. These functions only provide rough estimates and are not used in the present study. They are shown for comparative purposes in Fig. A1. The R package CoastalLight has been developed the present study to provide more accurate estimates (Section 5) calculated from the underlying data, that is the number of pixels and their size.

These changes in approach together with the different data sets used for the optical and bathymetric data have led to significant changes in three factors that affect bottom PAR (Fig. B1, Table 4). Two of them contribute to a decline of bottom PAR: a change in the depth distribution leading to an increase in the median depth (39 vs 31 m) and the distribution of $K_{d\ PAR}$ moved towards larger values in 2019. The third factor controlling PAR_{bottom} is surface PAR which tends to be higher in the present study than in the previous one. The combined effects of 1 and 2 are larger that the effect of 3, explaining why PAR bottom is overall smaller in the present study than in the previous one (Gattuso et al., 2006).

[**David A.: Que dire du traitement des données qui expliquerait que l'on a des KPAR et PAR plus élevés en 2019 qu'en 2006. ?**]

Table 4. Main characteristics of the products used by Gattuso et al. (2006) and the present study. **Bernard, peux-tu compléter?**

		Gattuso et al. (2006)	Present study
Depth (m)	Non polar	XX	XX
	Arctic	XX	XX
$K_{d\ PAR}$ (m^{-1})	Non polar	XX	XX
	Arctic	XX	XX
PAR ($\mathrm{mol\ photons\ m^{-2}\ d^{-1}}$)	Non polar	XX	XX
	Arctic	XX	XX

3.4 Implications for the distribution of photosynthetic organisms and communities

The differences in PAR_{bottom} between the 2006 study and the present one have implications of the potential surface areas receiving enough irradiance to sustain growth of photosynthetic organisms and communities (Table 5). Surface areas are 4 to 47% lower in the present study depending on the region and organism or community considered. As shown in Fig. 3, in the non polar region the highest the irradiance threshold, the largest the difference. Hence, the differences are generally reasonable (less than 15%) for organisms but higher (up to 47%) for communities which have higher light requirements to maintain rates of net primary production above 0. Differences between the 2006 estimates and the present ones are generally larger in the Arctic than in non the polar region for organisms and fairly similar for communities.

3.5 Analysis of time series

[**Les Davids**: pouvez-vous développer un peu cette section?]

Table 5. Top: Organisms. Surface area (% of the coastal zone) where irradiance does not limit the distribution of photosynthetic organisms. Values reported by Gattuso et al. (2006) are shown in parentheses for comparative purposes. The irradiance thresholds are the first deciles of the minimum light requirements compiled by Gattuso et al. (2006). Data are not reported in the Arctic region for seagrasses and Scleractinian (reef-building) corals where these groups are not present. **Bottom: Communities**. Surface area (% of the coastal zone) where benthic irradiance is higher that the daily community compensation irradiance (NPP>0). The irradiance thresholds are the first deciles of the minimum light requirements compiled by Gattuso et al. (2006). Data are not reported for seagrass communities and coral reefs in the Arctic and Antarctic regions where they do not occur.

		Percent surface area in region				
	Irradiance	Non-polar	Arctic	Antarctic	Total surface area (10^6 km^2)	
Organisms						
Seagrasses	1.3	20 (28)	–	–	3.78 (5.27)	
Macroalgae						
– Filamentous and slightly corticated filamentous	0.2	37 (42)	18 (26)	4	8.21 (9.50)	
– Corticated foliose, corticated and foliose	0.098	43 (47)	23 (30)	5	9.65 (10.68)	
– Leathery and articulated calcareous	0.040	50 (54)	29 (36)	6	11.28 (12.37)	
– Crustose	0.001	70 (66)	49 (51)	19	16.32 (15.55)	
Microphytobenthos	0.4	31 (37)	14 (22)	3	6.73 (8.31)	
Scleractinian corals	0.18	38 (43)	–	–	7.29 (8.09)	
Communities						
Seagrass beds	2.4	15 (23)	–	–	2.78 (4.32)	
Macroalgal communities	1.6	18 (26)	8 (13)	2	3.91 (5.71)	
Microphytobenthic communities	0.24	36 (41)	17 (25)	3	7.83 (9.19)	
Coral reefs	4.4	10 (19)	–	–	–	–

Long-term changes in the optical characteristics have recently been described. For example, using SeaWiFS monthly global ocean transparency data over Sept. 1997 to Nov. 2010, He et al. (2017) described a rapid decrease in global mean ocean transparency at a rate of -0.85 m yr^{-1} between 1997 and 1999, followed by a small increase with a rate of 0.04 m yr^{-1} over 2000–2010.

With a time series 20 years long, it is tempting to investigate whether long term changes in PAR$bottom$ can be identified. Fig. 4 shows the percent surface area of the coastal zone receiving 2 $\mathrm{mol\ photons\ m^{-2}\ d^{-1}}$ or more. There is a highly significant trend with an increase in percent surface area of 0.1% $\pm$ XX [**Bernard?**] per year. However, trends are highly variable during specific time periods corresponding to various sets of ocean color sensors.We conclude that no long-term trend in PAR_{bottom} can be identified in this data set.

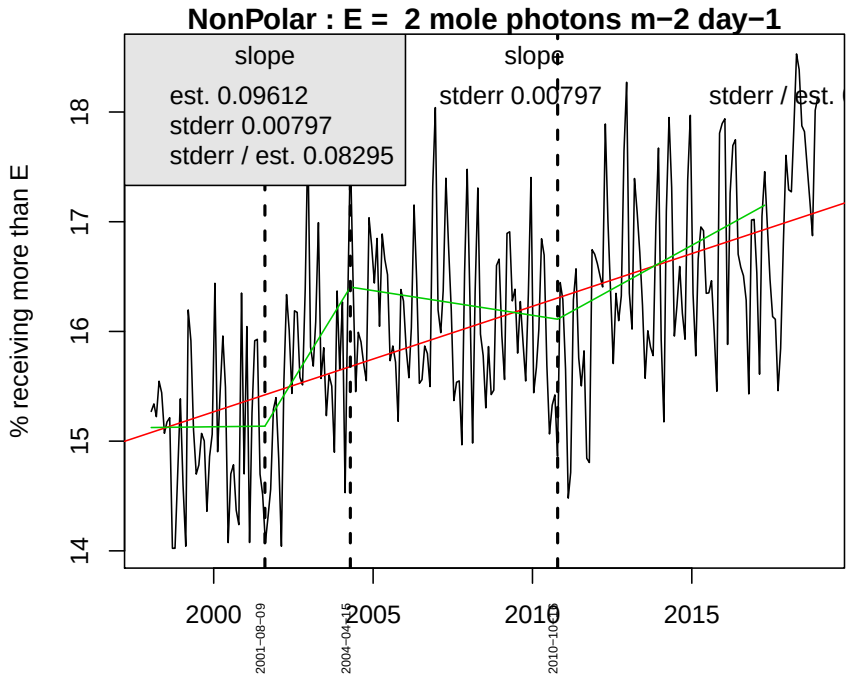

Figure 4. Time series of the surface area (%) of the coastal non polar region receiving more than 2 $\mathrm{mol\ photons\ m^{-2}\ d^{-1}}$. The linear regression over 1999-2018 is shown in red while the result of segmented regression over specific time periods corresponding to various sets of ocean color sensors is shown in green. Each period is delineated using vertical black dotted lines.

4 Conclusions

Light is a key variable controlling the distribution of benthic, photosynthetic organisms and communities. This study builds on the first, and still only, global distribution of photosynthetically available radiations (PAR) reaching the sea floor (Gattuso et al., 2006). It improve the quality, as well as geographical and depth resolutions, and cover a much longer period of time. Despite these key improvements, several limitations inherent to the approach remain. While the spatial resolution is twice better than the previous producst, at 4.6 km at the equator it is still very coarse for investigating the distribution and function of organisms and communities which change at a much finer scale. The parameterization used to convert reflectance data to irradiance is very approximate in case 2 water. Finally, light absorption by processes other than water column processes, for example the benthic nepheloid layer, are not taken into consideration. Nevertheless, the global distribution of PAR we provide is derived with state-of-the-art data and computations and is the best that can be offered at this time.

5 Data availability

The surface area of the coastal zone receiving an irradiance above a certain threshold is available for the Arctic, Antarctic and non-polar regions are available:

- from Pangaea: doi...
  - a netCDF file with geographical information (latitude, longiture, depth) (about 2 Gb)
  - a netCDF file with mean values of the 242 monthly data of PAR, KPAR and bottom irradiance (about 1.5 Gb)
  - 12 netCDF file with monthly mean of the 21 monthly values of PAR, KPAR and bottom irradiance (about 1.5 Gb each)
- from the R package Coastal Light... link to package, link to vignette

More

Appendix A: Graphical representation of P-functions

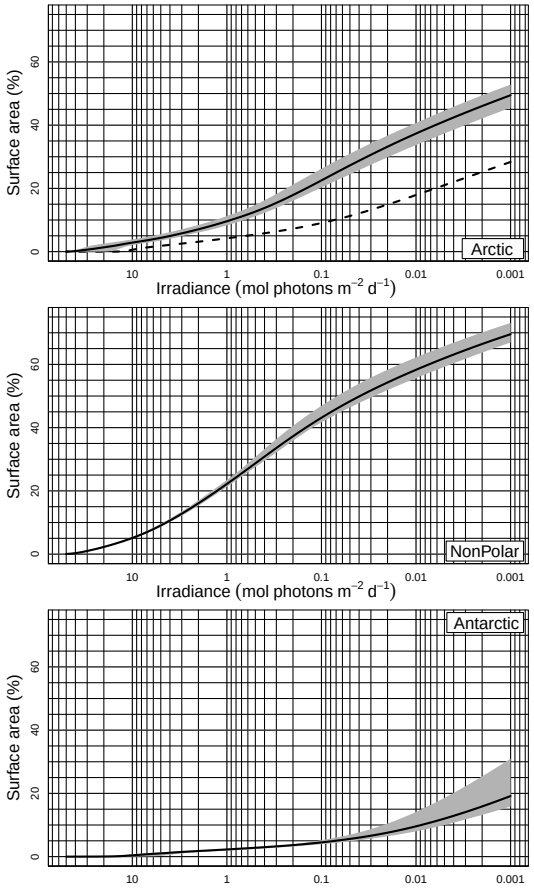

Figure A1. Cumulative surface area of the sea floor (S) receiving irradiance above a prescribed threshold (E_z). Data are expressed in percent of the total surface area of each region ($19,080,010$, $6,100,532$ and $146,171$ km^2, respectively for the non-polar, Arctic and Antarctic regions). The shaded area shows the monthly variability. [**Bernard: Note que le bas de la figure est coupé et qu'il faut enlever le trait pointillé dans l'Arctique**].

Appendix B: Distribution of depth, K_{dPAR} and PAR

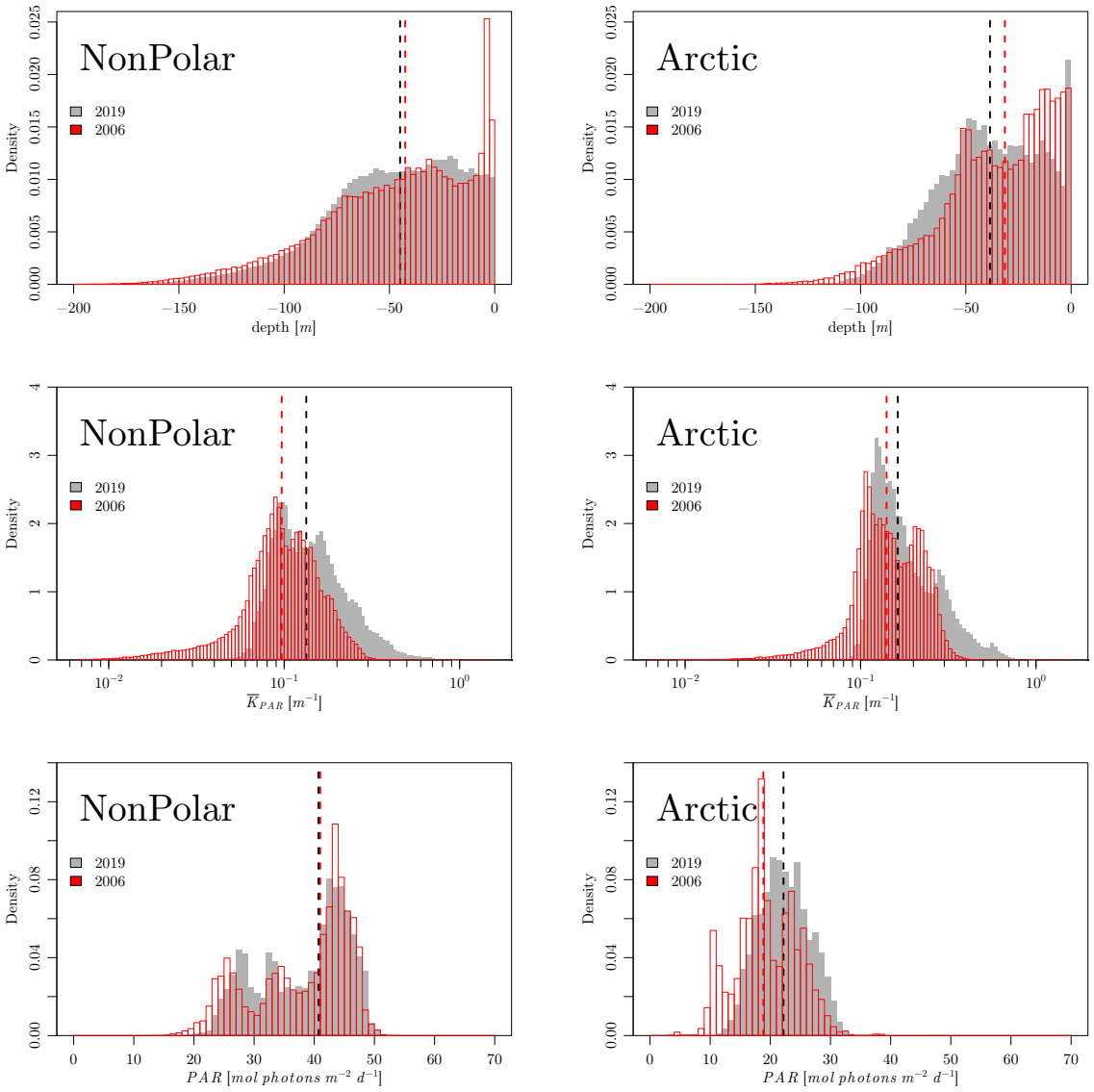

Figure B1. Distribution of depth, K_{dPAR} and PAR in the present study and in Gattuso et al. (2006). **Bernard: tu peux compléter ? median or mean? Je pense median c'est mieux**

Author contributions. JPG designed research and wrote the manuscript with contributions from BG, DA and DD. BG processsed the data and all authors contributed to the discussion of ideas.

Competing interests. None.

Acknowledgements. This is a product of The Ocean Solutions Initiative (http://bit.ly/2xJ3EV6), with support from Prince Albert II of Monaco Foundation, Veolia Foundation, IAEA Ocean Acidification International Coordination Centre and French Facility for Global Environment; and of the EU-H2020 project INTAROS (grant #727890).

References

ACRI-ST GlobColour Team: GLOBCOLOUR Product User Guide Version 4.1, ACRI-ST, 2017.

Antoine, D., André, J.-M., and Morel, A.: Oceanic primary production. 2. Estimation at global sclae from satellite (coastal zone color scanner) chlorophyll, Glob. Biogeochem. Cycles, 10, 43–55, 1996.

Assis, J., Tyberghein, L., Bosch, S., Verbruggen, H., Serrão, E. A., and Clerck, O. D.: Bio-ORACLE v2.0: Extending marine data layers for bioclimatic modelling, Glob. Ecol. Biogeogr., 27, 277–284, 2018.

Attard, K., Hancke, K., Sejr, M., and Glud, R.: Benthic primary production and mineralization in a High Arctic fjord: in situ assessments by aquatic eddy covariance, Mar. Ecol. Prog. Ser., 554, 35–50, 2016.

Capuzzo, E., Stephens, D., Silva, T., Barry, J., and Forster, R. M.: Decrease in water clarity of the southern and central North Sea during the 20th century, Glob. Change Biol., 21, 2206–2214, 2015.

Claustre, H. and Maritorena, S.: The many shades of ocean blue, Science, 302, 1514–1515, 2003.

Delesalle, B., Pichon, M., Frankignoulle, M., and Gattuso, J.-P.: Effects of a cyclone on coral reef phytoplankton biomass, primary production and composition (Moorea island, French Polynesia), J. Plankt. Res., 15, 1413–1423, 1993.

Duarte, C. M.: Reviews and syntheses: Hidden forests, the role of vegetated coastal habitats in the ocean carbon budget, Biogeosciences, 14, 301–310, 2017.

Eriander, L.: Light requirements for successful restoration of eelgrass (Zostera marina L.) in a high latitude environment - Acclimatization, growth and carbohydrate storage, J. Exp. Mar. Biol. Ecol., 496, 37–48, 2017.

Eyre, B. D., Santos, I. R., and Maher, D. T.: Seasonal, daily and diel N2 effluxes in permeable carbonate sediments, Biogeosciences, 10, 2601–2615, 2013.

Filbee-Dexter, K. and Scheibling, R. E.: Detrital kelp subsidy supports high reproductive condition of deep-living sea urchins in a sedimentary basin, Aquatic Biology, 23, 71–86, 2015.

Gattuso, J.-P., Gentili, B., Duarte, C., Kleypas, J., Middelburg, J., and Antoine, D.: Light availability in the coastal ocean: impact on the distribution of benthic photosynthetic organisms and their contribution to primary production, Biogeosciences, 3, 489–513, 2006.

Glud, R., Woelfel, J., Karsten, U., Kühl, M., and Rysgaard, S.: Benthic microalgal production in the Arctic: applied methods and status of the of the current database, Bot. Mar., 52, 559–571.

Gohin, F., Van der Zande, D., Tilstone, G., Eleveld, M., Lefebvre, A., Andrieux-Loyer, F., Blauw, A., Bryère, P., Devreker, D., Garnesson, P., Hernández Fariñas, T., Lamaury, Y., Lampert, L., Lavigne, H., Menet-Nedelec, F., Pardo, S., and Saulquin, B.: Twenty years of satellite and in situ observations of surface chlorophyll-a from the northern Bay of Biscay to the eastern English Channel. Is the water quality improving, Remote Sens. Environ., 233, 111 343, 2019.

He, X., Pan, D., Bai, Y., Wang, T., Chen, C.-T. A., Zhu, Q., Hao, Z., and Gong, F.: Recent changes of global ocean transparency observed by SeaWiFS, Cont. Shelf Res., 143, 159–166, 2017.

Krause-Jensen, D. and Duarte, C. M.: Substantial role of macroalgae in marine carbon sequestration, Nat. Geosci., 9, 737–742, 2016.

Krause-Jensen, D., Lavery, P., Serrano, O., Marbà, N., Masque, P., and Duarte, C.: Sequestration of macroalgal carbon: the elephant in the Blue Carbon room, Biol. Lett., 14, 20180 236, 2018.

Macreadie, P.: The future of Blue Carbon science, Nat. Comm., 2019.

Morel, A. and Bélanger, S.: Improved detection of turbid waters from ocean color sensors information, Remote Sens. Environ., 102, 237–249, 2006.

Morel, A. and Gentili, B.: Diffuse reflectance of oceanic waters.3. Implication of bidirectionality for the remote-sensing problem, Appl. Opt., 35, 4850–4862, 1996.

Morel, A., Huot, Y., Gentili, B., Werdell, P., Hooker, S., and Franz, B.: Examining the consistency of products derived from various ocean color sensors in open ocean (Case 1) waters in the perspective of a multi-sensor approach, Remote Sens. Environ., 111, 69–88, 2007.

Tyler, J.: The Secchi disk, Limnol. Oceanogr., 13, 1–6, 1968.

Weinberg, S.: Submarine daylight and ecology, Mar. Biol., 37, 291–304, 1976.

Wessel, P., Smith, W., Scharroo, R., Luis, J., and Wobbe, F.: Generic Mapping Tools: improved version released, Eos, Transactions American Geophysical Union, 94, 409–410, 2013.

Wilson, R. and Heath, M.: Increasing turbidity in the North Sea during the 20th century due to changing wave climate, Ocean Sci. Discuss., 2019.